# scientific reports

OPEN

# New Au/chitosan nanocomposite modified carbon paste sensor for voltammetric detection of nicotine

M. Shehata✉, M. Zaki & Amany M. Fekry

A profoundly touchy voltammetric sensor for detection of nicotine (NIC) in urine and tobacco specimens has been developed in light of the boosted electrochemical response of NIC at gold and chitosan nanocomposite modified carbon paste electrode (ACMCPE). Material characterization techniques Scanning Electron Microscope and Energy Dispersive X-ray (SEM & EDX) were utilized to describe the ACMCPE surface material. The impedance spectroscopy technique (EIS), cyclic voltammetry (CV), chronoamperometry (CA), and differential pulse voltammetry (DPV) were employed to explore the electrochemical sensing of NIC at ACMCPE. The created sensor exhibits an exceptional electrochemical sensitivity to NIC in a universal Britton–Robinson (B-R) buffer solution with a pH range of 2.0 to 8.0. The sensor shows a linear response over NIC concentration ranges of 4.0–320.0 μM, with the detection limit (LOD) of 7.6 μM. The prepared sensor has been shown to be exceptionally viable in detecting NIC with amazing selectivity and reproducibility. We suggest it as a trustworthy and useful electrochemical sensor for NIC location.

NIC is perhaps of the most well-known normal alkaloid, and it's the primary component in tobacco plants that is generally used to produce cigarettes[1,2]. When consumed through smoking, this substance might cause different adverse consequences on human health, involving elevated blood pressure and heart rate, as well as central nervous system excitement[3–7]. Thus, from a toxicological and medical standpoint, checking NIC levels is mandatory. Numerous techniques have been utilized to detect NIC in the human body or tobacco specimens, including spectrophotometry[8], HPLC technique[9], gas chromatography[10] and capillary electrophoresis[11]. Some of these approaches, however, have shortcomings, such as the need of sample pretreatment, expensive prices, and long processing time. Electroanalytical strategies, which can give high awareness, fast response, simplicity of activity, and minimal expense, are ideal options in this regard[12–14]. Nanomaterials have been generally utilized in sensors and biosensors because of their novel properties, for example, the presence of conduction centers, facilitating electron transfer and providing large catalytic surface areas, as well as enhanced diffusion and adsorption towards target molecules. In recent years, various nanomaterials for electrode surface modification have been reported[15–18]. One of the new encouraging materials, Au nanoparticles (Au-NPs), were generally used to improve electrodes. This choice was made essentially as a result of Au-NPs have consistent physical and chemical resources, useful catalytic activities, and little dimensional size[19,20]. Based on these advantages, it has been proved that, modifying carbon paste electrodes (CPEs) with Au-NPs improves sensitivity of the electrode, facilitates charge transfer, and lowers the analyte detection limit. For example, Afkhami et al.[21] developed a sensor that detects cefixime in urine and pharmaceutical samples using a multi walled CPE (Au-NPs/MWCPE) modified with Au-NPs. The benefits of this sensor are its extremely low detection threshold, elevated sensitivity, and outstanding stability. Arvand et al.[22] developed a sensor for measuring folic acid in human blood plasma using an Au-NPs-modified CPE. This sensor has a fast response time and a high sensitivity. Recently, a few investigations on the detection of NIC utilizing Au-NPs nanoparticles have been conducted. For instance, Saljooqi et al.[23] reported electrocatalytic action of the composite GCE/GO, and polythiophene (PT) decorated with Au-NPs enabling anodic peak current of NIC oxidation to be noticed at the potential of + 0.81 V and limit of detection $1.7 \times 10^{-7}$ mol mL$^{-1}$. Whilst, Jing et al.[24] have revealed a detection limit of 0.015 μM at PDA-RGO/Au nanocomposite sensor in tobacco products. More recently, the synthesis of nanocomposite of Au-NPs with chitosan has received a lot of interest. Chitosan, a deacetylated derivative of chitin, is rich in amino groups as

Chemistry Department, Faculty of Science, Cairo University, Giza 12613, Egypt. ✉email: Mshehata@cu.edu.eg; Mshehata@sci.cu.edu.eg; Mohammed.shehata9011@yahoo.com

being a linear polysaccharide, exhibits good biocompatibility, owing prominent electronic properties and has an excellent stability which allows good electrocatalytic activity, large specific surface area and high sensitivity towards NIC when combined with the well biocompatible Au-NPs. The strong interest in this polymer stems from its appealing features, which include outstanding high-water permeability, strong adhesion, and film-forming properties, and chemical modification susceptibility as a result of the existence of reactive amino and hydroxyl functional groups[25–29]. These functional groups could contribute to the settlement of Au-NPs on the surface of the electrode as well as the electrode surface's catalytic activity. Zhang et al.[30] constructed a sensor based on chitosan and Au-NPs. They found that chitosan averted the agglomeration of the Au-NPs as well as maintained the stability of nanoparticles. For the creation of electrochemical sensors, it is in fact especially appealing to create hybrid materials that combine highly conductive Au-NPs with a wide range of organic functional groups capable of selectively interacting with target molecules. In earlier works, two highly sensitive NIC detection sensors using CPE modified with Ni/Cu NPs and Mn/Cu NPs have been constructed by M. Zaki et al.[31,32]. In this work, a novel NIC sensor with outstanding detection properties was created by electrodepositing Au -NPs onto a chitosan/CPE surface.

## Experimental

### Reagents and solutions

The standard NIC analyte sample (99%) was supplied by the Egyptian Smoking Eastern Company and was used without prior refinement. The freshly made 1.62 g L$^{-1}$ NIC stock solutions in water were then stored in a dark container due to the compound's light sensitivity. Paraffin oil mixed with graphite fine particles, supplied by Merck, were used to set up the CPE. Gold chloride salt ($KAuCl_4$) and chitosan powder were provided by Aldrich (USA). (B–R) buffer solutions ($4.0 \times 10^{-2}$ M), utilized as supporting electrolytes, were prepared from $CH_3COOH$, $H_3BO_3$ and $H_3PO_4$ at pH values ranging from 2.0–8.0. PH values were changed utilizing HCl (0.2 M) and NaOH (0.2 M). Each experiment produced repeatable findings after being run two to three times at laboratory room temperature.

### Modified electrodes construction

A homogenous paste was made by mixing 2 mL of paraffin oil with 5.0 g of graphite powder in a mortar for 5 min to prepare the bare carbon paste electrode (denoted as BCPE)[33,34]. In order to find the optimal sensor composition, several attempts were made to create the modified CPE with chitosan by mixing various amounts of chitosan into the paste and assessing their response toward NIC. On that principle, 0.4 g of CP and 0.1 g of chitosan powder were prepared to create a Chitosan/CPE (denoted as CCPE). Every composite combination was then stuffed into the finish of a Teflon tube (a hole of 3 mm in diameter which equals 0.0706 cm$^2$ electrode surface area) and polished with ultrafine emery paper to obtain a smooth surface. In order to prepare the Au-NPs/Chitosan/CP electrode (denoted as ACMCPE), the CMCPE was submerged in a solution of gold chloride (0.01 M) for 300 s to deposit Au-NPs on the surface of the CMCPE at a deposition potential of -0.4 V. It was then dried for 5 min by air.

### Cell and devices

The electrochemical investigations were carried out at room temperature using a three-electrode cell with a capacity of 25 mL, consisting of an ACMCPE as the working electrode, a platinum auxiliary electrode (CE), and a calomel reference electrode (RE). Electrochemistry techniques such as DPV, CV, CA and EIS were carried out by SP-150 potentiostat connected to the EC-Lab® software package. EIS measurements were carried out at 10 mV ac amplitude in the frequency range of 1.0 mHz to 100 kHz. EC-Lab® programming was utilized to fabricate the best comparable circuit models[35–37]. pH measurements were performed using a pH-meter from Hanna Instruments in Italy. Energy Dispersive X-ray analyzer (Bruker) and SEM (TESCAN VEGA3, Czech Republic) were used to evaluate the electrode's surface morphology. Transmission electron microscopy (TEM) analysis was made using a JEM-1400 Electron Microscope (JEOL, Japan).

### Analysis of urine

Real urine samples were examined using a diluted pee solution created by diluting 400 times in 100 mL of B-R buffer pH 2 in order to create a stock solution. A solution containing NIC in B-R buffer at pH = 2 was used to establish standard increments of NIC at different concentrations to get the calibration graph.

### Cigarette sample examination

Cigarettes were dried for 30 min on a 40 °C stove after being taken out of their rolling papers. 10 mL of water and 0.1 g of tobacco from a combination of 10 cigarettes (from two packs of a comparable brand) were added, and the mixture was then sonicated for 3 h in an ultrasonic water bath and filtered. The B-R buffer (pH 2.0) was mixed with the appropriate volume (100 mL) of the filtrate and evaluated under the same conditions as those used to obtain the calibration graph[5].

## Results and discussion

### Morphology of the investigated electrodes

SEM micrographs were used to examine the surface morphology of the Au-NPs that had been deposited on Chitosan/CPE. The Au-NPs have an approximately spherical shape and are dispersed randomly at varying altitudes over the electrode surface, as indicated by the SEM images of the ACMCPE surface at several amplifications shown in Fig. 1a–c. This suggests a significant surface area. According to the scale of the image, the
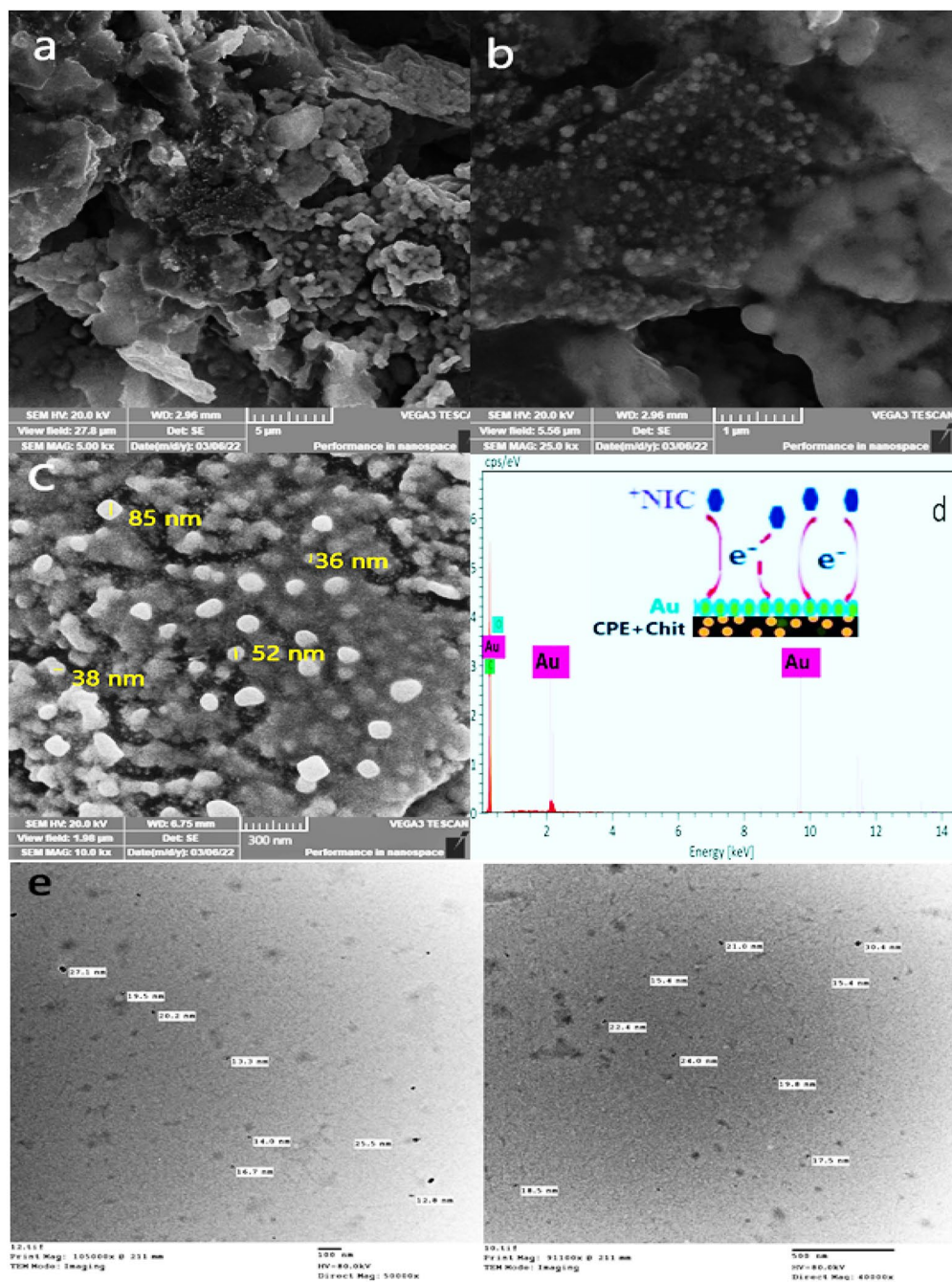
**Figure 1.** ACMCPE SEM pictures (**a**–**c**) at various amplifications. (**d**) EDX spectra of ACMCPE surface including NIC/ACMCPE interaction model. (**e**) Transmission electron microscopy (TEM) micrograph of Au nanoparticles.

size of Au-NPs varies between 30 and 50 nm as depicted in Fig. 1c. Only 85 nm particle was odd one and not repeatable across the whole prepared surface, which enhanced our surface stability and its well preparation procedure. Also TEM images enhanced our findings and the sizes were nearly from 15–30 nm as reported in Fig. 1e. The different particle sizes observed might be explained by nucleation, agglomeration, and subsequent growth. The EDX analysis of the ACMCPE sensor is shown in Fig. 1d, which verifies the presence of C, O, and Au by a percentage of 84.57%, 1.09%, and 14.34% respectively, confirming that Au-NPs were indeed coated on the Chitosan /CPE surface.

## Electrochemical measurements

The CV and EIS were used to evaluate the electrochemical properties of NIC at CPE, CCPE, and ACMCPE. Figure 2A shows typical voltammograms of 1.0 mM NIC in a B-R buffer (pH 2) produced by scanning the three
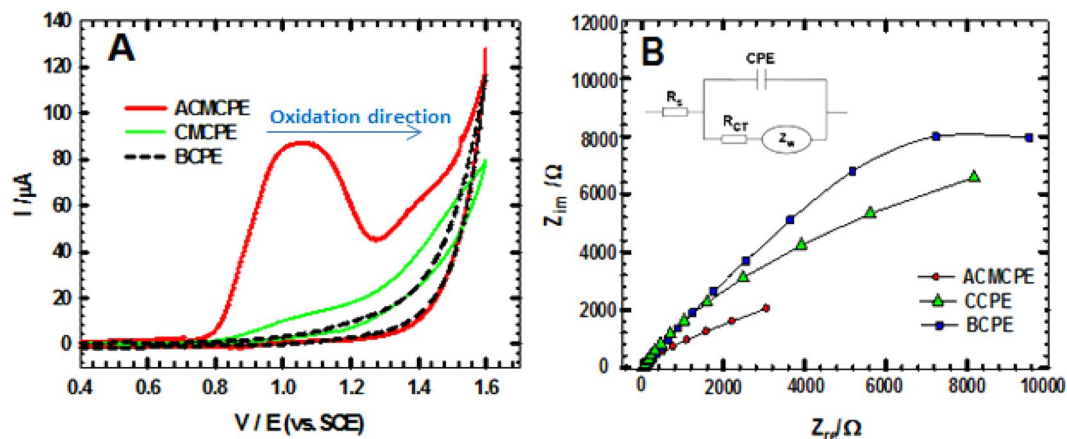
**Figure 2.** (**A**) CVs of BCPE, CCPE and ACMCPE at $\nu = 50$ mV s$^{-1}$ in 1 mM NIC utilizing B-R buffer (pH 2). (**B**) Nyquist plots for BCPE, CMCPE and ACMCPE in 1 mM NIC using B-R buffer pH 2. Inset: equivalent circuit model.

working electrodes at a rate of 50 mV s$^{-1}$. The oxidation of NIC at ACMCPE results in an irreversible oxidation peak (voltammogram ACMCPE) at + 1050 mV and Ip = 82.35 μA. In contrast, no redox response was observed for BCPE and a small Ip = 8.9 μA at a potential of around + 1000 mV was observed for CCPE, suggesting that the electrodeposition of Au-NPs on to the surface of the chitosan/CPE was a successful technique for improving NIC detection.

The Randles–Sevcik equation[38–40] was utilized to determine the active surface area of the modified electrode for a known $K_4[Fe(CN)_6]$ concentration:

$$Ip = 2.69 \times 10^5 \, n^{3/2} \, A \, D^{1/2} \, \nu^{1/2} \, C, \tag{1}$$

where Ip is the peak current (A), $\nu$ is the scan rate (V s$^{-1}$), A is the electrode area, n is the number of transferred electrons, D the diffusion coefficient which equals to $7.6 \times 10^{-6}$ cm$^2$ s$^{-1}$, and C is the concentration of $K_4[Fe(CN)_6]$. For 1.0 mmol L$^{-1}$ $K_4[Fe(CN)_6]$ in 0.10 mol L$^{-1}$ KCl electrolyte with n = 1.

The bare electrode area was calculated using the hole diameter of 3 mm using $\pi r^2 = 0.0706$ cm$^2$ and after deposition of Au-NPs, the active surface area of ACMCPE was increased to 0.144 cm$^2$.

Nyquist plots were exhibited at + 1050 mV ($E_p$ from CV) for ACMCPE, CCPE, and BCPE (Fig. 2B). In the high-frequency region, the semicircle diameter of EIS corresponds to the charge transfer resistance ($R_{CT}$) at the electrode electrode/electrolyte interface. A comparison of the semicircular regions of the three EIS curves at high frequency shows that the modified electrode ACMCPE has a lower $R_{CT}$ than the bare electrode and CCPE[41–43]. The Randles circuit model was used to fit the acquired EIS curve (Fig. 2B inset) including $R_{CT}$, solution resistance ($R_s$), constant phase element of capacitance (CPE) and Warburg impedance ($Z_w$)[44–46]. The fitting was done with EC-Lab® software supplied with the SP-150 workstation. The ACMCPE electrode was shown to have higher values for $Z_w$ (1380 Ω cm$^2$ s$^{-1/2}$), CPE (18.7 μF cm$^{-2}$), and a lower value for the $R_{CT}$ (2243 Ω cm$^2$) demonstrating greater conductivity than bare CPE and CCPE with CPE = 6.3 μF cm$^{-2}$, W = 456 Ω cm$^2$ s$^{1/2}$ and $R_{CT}$ = 12,960 Ω cm$^2$ and CPE = 8.6 μF cm$^{-2}$, W = 488 Ω cm$^2$ s$^{-1/2}$ and $R_{CT}$ = 11,250 Ω cm$^2$ respectively. Accordingly, the considerable decrease in $R_{CT}$ for ACMCPE compared to BCPE and CCPE can be attributed to Au-NPs deposited on CMCPE, which forms many electrocatalytic centers, lowering the contact resistance between ACMCPE/electrolyte interfaces. These findings back up the high anodic current $I_p$ value obtained from CVs for ACMCPE electrodes.

### Influence of pH

The cyclic voltammogram approach was used to assess the impact of pH on NIC oxidation peak utilizing B-R buffer (pH 2–8) at both the BCPE and ACMCPE. According to Fig. 3, the anodic Ep moved negatively with rising pH values, demonstrating that protons are involved in electrode reactions and that the electrocatalytic oxidation of NIC was a pH-dependent process[47–49]. In addition, the linear relationship between Ep for NIC oxidation and pH (Ep = − 0.06 pH + 1.16 (R$^2$ = 0.99) was demonstrated (see Fig. 3 inset B). According to the slope value, the electrode reactions demand an equal number of electrons and protons. At acidic and basic media, it is also obvious that peak potential varies with pH. At pH 2, the maximum peak current signal was obtained, which gradually decreased from 2.0 to 6.0 before increasing at pH 8. Accordingly, depending on the pH of the media, NIC has two pKa values: 3.12 and 8.02, which are equivalent to the monoprotonated (protonation of pyrrolidine nitrogen) and diprotonated (pyridine nitrogen) forms of the NIC molecule, respectively[50,51]. These results could indicate that NIC oxidation took place via protonation of nitrogen atoms on the pyrrolidine ring and was assigned to tertiary nitrogen oxidation.

Figure 4 shows Nyquist plots of NIC at different pH values utilizing ACMCPE at $E_p$ vs. SCE. The EIS results are consistent with those obtained from CV. At different pH solutions, the Nyquist plot of ACMCPE shows almost straight lines at lower frequencies and tiny incomplete semicircles at higher frequencies, which correspond to
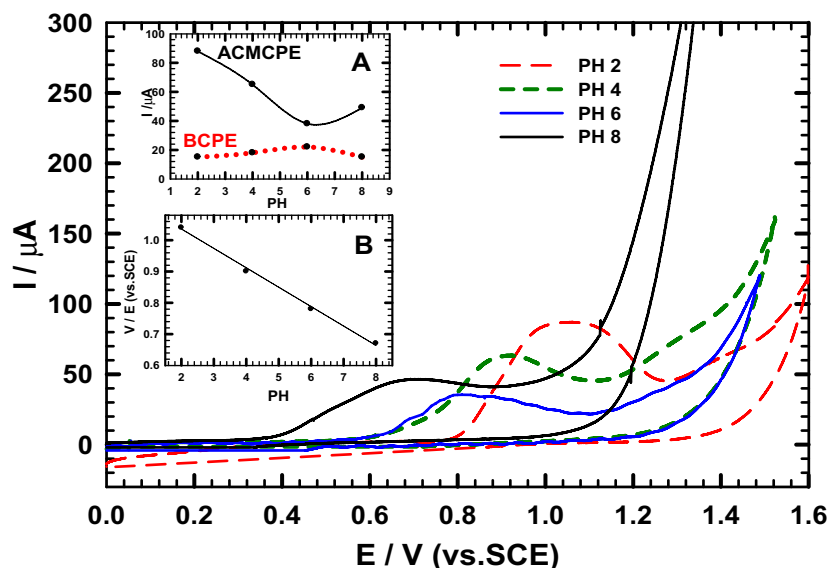
**Figure 3.** CVs of NIC at 50 mV s$^{-1}$ using ACMCPE at different pH levels in B-R buffer. Inset: (**A**) A plot of pH vs. $I_{pa}$ at BCPE and ACMCPE. (**B**) A plot of Ep vs. pH at ACMCPE.
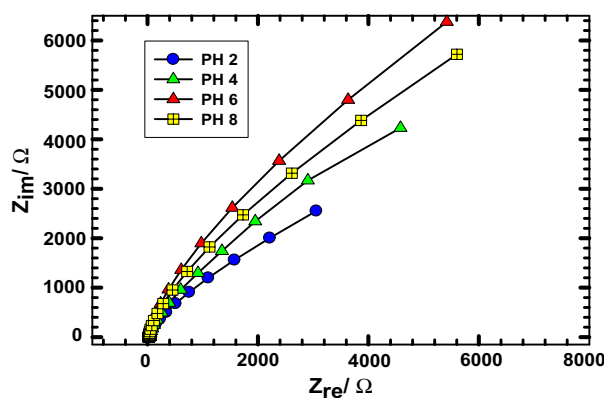


**Figure 4.** Nyquist plots of 1 mM NIC in various pH values utilizing ACMCPE.

diffusion-limited and electron transfer-limited processes[52–54]. The Nyquist plot at pH 2 shows a substantially smaller semicircle in the high-frequency region than other pH solutions, implying that ACMCPE at pH 2 has greater electron transport capabilities.

### The influence of scan rate

In order to investigate the kind of the electrochemical process on the ACMCPE electrode, the impact of the scan rate (v) on the electrooxidation of NIC ($1 \times 10^{-3}$ M) was studied at various scan rates ranging from 10 to 200 mV s$^{-1}$ using CV in B-R buffer (pH 2). It is clear that, in Fig. 5, as the scan rate increased, the peak potential (Ep) of the oxidation of NIC went considerably to higher positive values, demonstrating the irreversibility of the reaction[55,56]. A plot of the anodic peak currents (Ip) and the square root of scan rate (v$^{1/2}$) revealed good linearity (Ip = 15.2 × v$^{1/2}$ + 20.6) with a correlation coefficient of r$^2$ = 0.988 (see Fig. 4 inset), indicating that the charge transfer was a diffusion-controlled process[57,58]. In addition, the diffusion coefficients, $D_{app}$, of NIC in B–R buffer (pH 2.0) utilizing ACMCPE and CMCPE were derived from the relationship between the squire root of the scan rate v$^{1/2}$ and the anodic peak current $I_{pc}$ (A) [Fig. 5 inset] based on the Randles–Sevcik equation[59–61].

$$I_p = 0.4463\, nFAC_0\, (nFvD/RT)^{1/2}. \tag{2}$$

In this equation, n is the number of electrons exchanged in oxidation at T = 298 K, $C_0$ is the analyte concentration ($1 \times 10^{-6}$ mol cm$^{-3}$), D is the electroactive species diffusion coefficient (cm$^2$ s$^{-1}$), F is the Faraday constant in C mol$^{-1}$, v is the scan rate in V s$^{-1}$, A is the geometrical electrode area (cm$^2$), and R is the gas constant in VC
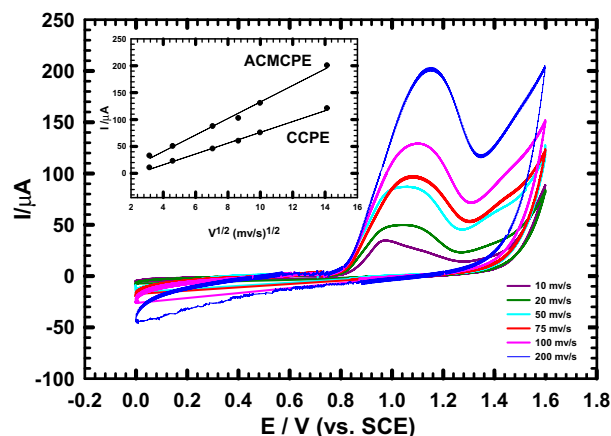
**Figure 5.** Influence of changing the scan rate ν from (10–200) mV s$^{-1}$ on I$_{pa}$ response of 1 mM NIC in B-R buffer (pH 2). Inset: Plot of the anodic peak currents Ip vs. ν$^{1/2}$ for ACMCPE and CCPE.

K$^{-1}$ mol$^{-1}$. Thus, the apparent diffusion coefficients, D$_{app}$, of NIC at ACMCPE and CMCPE were found to be $8.841 \times 10^{-5}$ cm$^2$ s$^{-1}$ and $5.12 \times 10^{-5}$ cm$^2$ s$^{-1}$, respectively.

### Chronoamperometry

The chronoamperometric response of NIC in B-R buffer (pH 2.0) was recorded at a constant potential (+ 1050 mV vs. SCE) utilizing ACMCPE sensor. The NIC calibration graph, shown in Fig. 6 inset B, was created by plotting NIC concentrations versus oxidation currents at a given time (1 s). A linear relationship was observed from 20 to 600 μM with a linear equation of Ip = 0.062 C + 15.74, and a correlation coefficient of 0.96. Based on the Cottrell equation[62–64], the diffusion coefficient can be calculated from the equation.
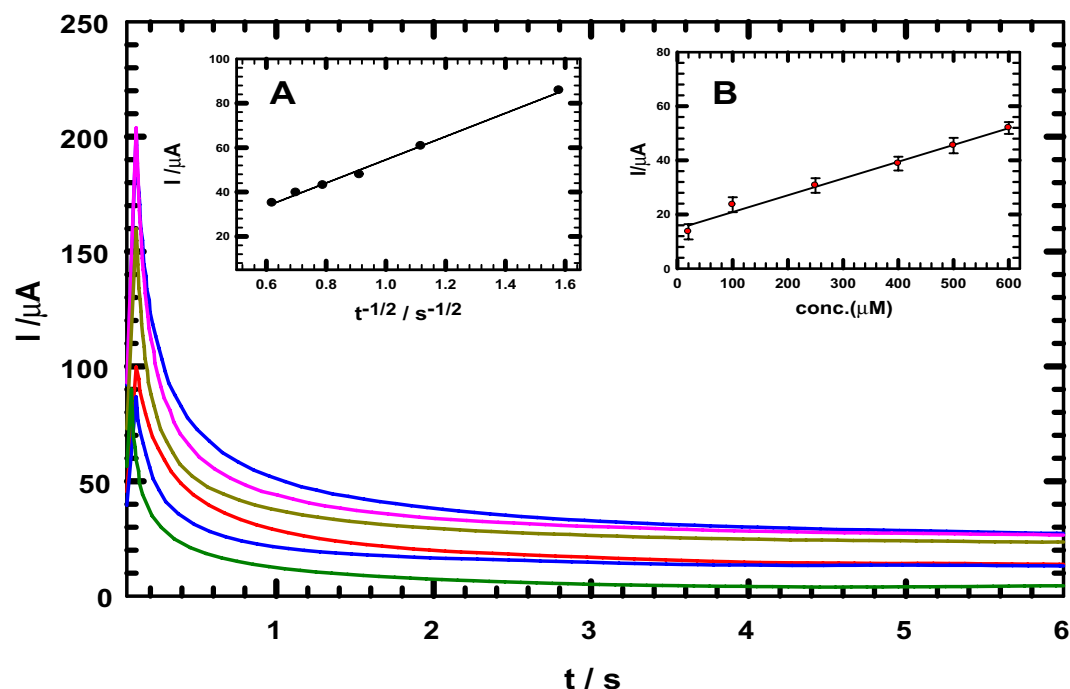


**Figure 6.** Chronoamperograms obtained at ACMCPE with varying doses of NIC (20, 100, 250, 400, 500, and 600 μM) in B-R buffer pH 2. Inset: (**A**) I vs. t$^{-1/2}$ figure obtained from 600 μM NIC chronoamperogram. (**B**) Calibration plot for various NIC concentrations at a given period of 1 s. Error bars represent the standard deviations of three repetitive tests.

$$i = \left[ \frac{nFAc^0\sqrt{D}}{\sqrt{\pi t}} \right], \qquad (3)$$

where i = current, in unit A, F = Faraday constant (96,485 C/mol), n = number of electrons, $c^0$ = bulk concentration of the analyte in mol/cm³; A = area of the electrode in cm², D = diffusion coefficient for species in cm²/s and t = time in s. The slope obtained from the relationship between the anodic peak current and $t^{-1/2}$ (Fig. 6 inset A) equals $nFAc^o(D/\pi)^{1/2}$, in accordance with the Cottrell equation, so the diffusion coefficient of NIC was calculated to be $7.38 \times 10^{-5}$ cm² s⁻¹. The NIC oxidation reaction is shown to be controlled by a diffusion control process, since the diffusion coefficient values estimated from chronoamperometric measurements (CA) are equivalent to those calculated from CV measurements.
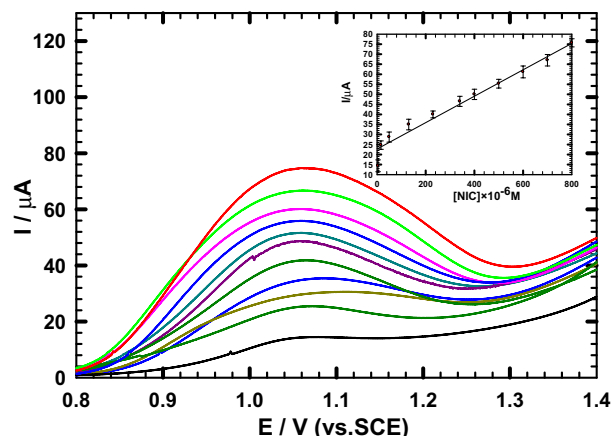
### Calibration plot

The DPV response of ACMCPE electrode to different NIC concentrations in B-R Buffer (pH 2) was measured at 10 mV s⁻¹, (Fig. 7). A distinct response was noted with the sequential addition of NIC, as indicated in Fig. 7. These results reveal that Au-NPs coated on a chitosan/CPE surface have a stable and efficient catalytic capability. Under optimal conditions, the response currents and NIC concentrations have a linear relationship in the range $4 \times 10^{-6}$–$3.2 \times 10^{-4}$ M. The plot of anodic peak currents vs. NIC concentrations (see Fig. 7 inset) demonstrated a linear regression with the following equation: Ipa (A) = 0.065 C + 22.76 and $r^2 = 0.96$. The following equations have been used to calculate the limits of detection (LOD) and quantification (LOQ):

$$LOD = 3s/m \qquad (4)$$

$$LOQ = 10s/m, \qquad (5)$$

where m is the slope (μA/M) of the calibration curves and s is the standard deviation (SD) (three runs); they were found to be $7.6 \times 10^{-6}$ M and $2.3 \times 10^{-6}$ M, respectively[65,66].

Comparisons of data acquired for determination of NIC using different instruments and electrochemical approaches versus ACMCPE were recorded in Table 1. Although it has roughly the same specific selectivity, the sensor has the benefit of employing non-poisonous and less expensive reagents. The ACMCPE sensor is less sophisticated and expensive than spectrometry equipment, HPLC, GC, and flow injection. Additionally, the



**Figure 7.** Effect of NIC addition in B-R buffer (pH 2.0) sequentially utilizing ACMCPE at 10 mV s⁻¹. Inset: NIC calibration curve utilizing ACMCPE. The standard deviations of three repeated tests are shown as error bars.

| Method | Calibration range (M) | Detection limit (M) | Reference |
|---|---|---|---|
| Cho enzyme biosensor | $9.2 \times 10^{-5}$–$2.0 \times 10^{-4}$ | $1.0 \times 10^{-5}$ | [49] |
| p-(AHNSA/GCE) | $0$–$5.0 \times 10^{-3}$ | $0.87 \times 10^{-6}$ | [67] |
| TiO2/MI-PEDOT | $0$–$5.8 \times 10^{-2}$ | $4.9 \times 10^{-6}$ | [68] |
| Pencil graphite electrode | $7.0 \times 10^{-6}$–$1.07 \times 10^{-4}$ | $2.0 \times 10^{-6}$ | [5] |
| CNMCP sensor | $4.0 \times 10^{-6}$–$5.0 \times 10^{-4}$ | $0.94 \times 10^{-9}$ | [65] |
| MCMCPE sensor | $2.0 \times 10^{-6}$–$6.0 \times 10^{-4}$ | $1.15 \times 10^{-7}$ | [31] |
| ACMCPE sensor | $4.0 \times 10^{-6}$–$3.2 \times 10^{-4}$ | $7.6 \times 10^{-6}$ | This work |

**Table 1.** Contrasting the recommended method with other techniques and electrodes for NIC measurement.

pre-treatment and processes for these technologies are challenging, in contrast to how easy and uncomplicated they are for the ACMCPE sensor.

### Interference study, reproducibility and stability

The interference effect on the voltammetric response for NIC was used to inspect the selectivity of the constructed sensor. It was tested in the presence of caffeine, ascorbic acid, uric acid, sucrose, lactose, and glucose, which are common in human urine and can interfere with NIC. The voltammetric response of various interferants was measured at anodic peak of Ep = + 1050 mV, with essentially negligible current response. Due to the low concentration of other minor alkaloids (0.2–0.5 percent of total alkaloids), which cannot affect the precision of NIC detection at the sensitivity level of voltammetric tests, the interference of alkaloids that may be present in tobacco was not addressed in this work. Because cotinine and NIC are structurally related, using them together would completely define the selectivity of the proposed sensor. A constant concentration of NIC (500 μM) was spiked with similar and two-fold concentrations of the NIC biomarker "cotinine". The same experimental settings were applied for CV measurements, and recovery data ranging from 99.3% to 100% were obtained, suggesting that the modified ACMCPE might be a useful electrocatalytic sensor for detecting NIC while avoiding interference. The sensor's reproducibility was assessed by contrasting the current responses of five independent constructed ACMCPEs for 100 μM NIC. It gives a similar result, with a variation of only 4.6%. This confirms that the preparation process of the electrode is highly reliable and consistent. The long-term stability of one electrode was also tested by determining its current response every three days; the electrode was kept in the air. After two weeks, the response is 95% of its initial value, and then drops to 90% after three weeks, indicating a relatively consistent performance for NIC detection.

### Actual samples study

*Usage of the ACMCPE sensor in urine*
In order to determine the methodology's applicability, the ACMCPE sensor was utilized to count the concentrations of NIC in urine samples. The calibration plot, shown in Fig. 8, produced a straight line that obeyed the linear relationship with $r^2 = 0.968$, $I_{pa}$ (μA) = 0.074 C + 17.05, and a LOD of 2.07 μM. On the calibration plot, four separate concentrations are chosen, and each is repeated five intervals to reveal the procedure's accuracy and precision. The concentration recovery was judged to be between 96.0–100.6% as shown in Table 2.

*Examination of real cigarettes samples*
To guarantee that the suggested procedure was validated with actual samples, two products from different cigarette products (Marlboro and L&M) were examined for a real application. This study employed a slightly amended version of the procedure supplied by Suffredini et al.[49]. To acquire the NIC value of the tobacco sample, an appropriate amount of standard NIC solution generated in the supporting electrolyte was added to the previously
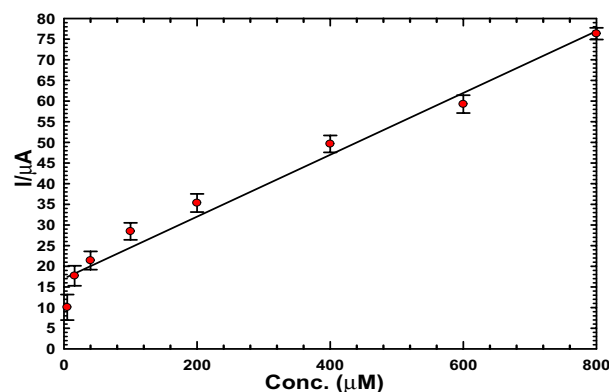


**Figure 8.** NIC calibration curve in urine.

| (NIC) taken × 10⁻⁶ M | (NIC) founded[a] (M) × 10⁻⁶ | Recovery | RSD % |
|---|---|---|---|
| 10 | 9.6 | 96.0 | 4.7 |
| 40 | 38.8 | 97 | 3.3 |
| 120 | 118.5 | 98.7 | 2.1 |
| 200 | 201.2 | 100.6 | 1.6 |

**Table 2.** The ACMCPE sensor's accuracy and precision for NIC detection in a urine sample. [a]Mean for five determinations.

| Cigarette brand | [NIC] taken $\times 10^{-6}$ M | [Standard] added $\times 10^{-6}$ M | Found $\times 10^{-6}$ M | Recovery (%) | RSD % |
|---|---|---|---|---|---|
| Marlboro | 40 | 40 | 78.3 | 97.8 | 3.8 |
| | 80 | – | 119.2 | 99.3 | 1.3 |
| | 120 | – | 161 | 100.6 | 2.2 |
| | 160 | – | 201 | 100.5 | 1.7 |
| L&M | 40 | 40 | 79.2 | 99 | 2.6 |
| | 80 | – | 121.5 | 101.25 | 2.4 |
| | 120 | – | 161.2 | 100.75 | 1.8 |
| | 160 | – | 200.9 | 100.45 | 1.4 |

**Table 3.** NIC recovery analysis in cigarette tobacco.

formed NIC content. The recommended method's ability to quantitatively recover NIC quantities demonstrates the accuracy of the NIC detection in tobacco. The recovery data supports this assertion. (See Table 3).

## Conclusions

In this study, we constructed a novel NIC sensor by electrodepositing Au-NPs onto a chitosan/CPE surface. This sensor showed outstanding NIC sensing performance due to the increase in the electro-active area developed by Au-NPs as revealed by the CV and EIS experiments. In the electrochemical NIC response, it showed a wide linear detection range ($4 \times 10^{-6}$–$3.2 \times 10^{-4}$ M) with a limit of detection $7.6 \times 10^{-6}$ M. The sensor has a good selectivity, sensitivity, and stability for NIC determination. Interference of any accompanying substrates wasn't detected. Additionally, it has been demonstrated that the sensor can accurately identify NIC in both urine and cigarette samples. As suggestion for future, a transfer from the success of NIC detection to cotinine detection based on ACCMCPE will broaden the analytical applications as Cotinine is the metabolite of NIC and structurally similar to it. Also screen printed electrode or any other graphite derivatives as carbon nanotubes, graphene or graphene oxide for NIC detection may be applied in future investigations.

## Data availability

The datasets used and/or analysed during the current study available from the corresponding author on reasonable request.

## References

1. Lin, B. *et al.* A facile approach for on-site evaluation of nicotine in tobacco and environmental tobacco smoke. *ACS Sensors* **4**, 1844–1850 (2019).
2. Stočes, M. & Švancara, I. Electrochemical behavior of nicotine at unmodified carbon paste electrode and its determination in a set of refilling liquids for electronic cigarettes. *Electroanalysis* **26**, 2655–2663 (2014).
3. Lloyd, G. K. & Williams, M. Neuronal nicotinic acetylcholine receptors as novel drug targets. *J. Pharmacol. Exp. Ther.* **292**, 461–467 (2000).
4. Jha, P. Avoidable global cancer deaths and total deaths from smoking. *Nat. Rev. Cancer* **9**, 655–664 (2009).
5. Levent, A., Yardim, Y. & Senturk, Z. Voltammetric behavior of nicotine at pencil graphite electrode and its enhancement determination in the presence of anionic surfactant. *Electrochim. Acta* **55**, 190–195 (2009).
6. Domino, E. F. Tobacco smoking and nicotine neuropsychopharmacology: Some future research directions. *Neuropsychopharmacology* **18**, 456–468 (1998).
7. Heeschen, C. *et al.* Nicotine stimulates angiogenesis and promotes tumor growth and atherosclerosis. *Nat. Med.* **7**, 833–839 (2001).
8. Figueiredo, E. C., de Oliveira, D. M., de Siqueira, M. E. P. B. & Arruda, M. A. Z. On-line molecularly imprinted solid-phase extraction for the selective spectrophotometric determination of nicotine in the urine of smokers. *Analytica Chimica Acta* **635**, 102–107 (2009).
9. Doctor, P., Gokani, V., Kulkarni, P., Parikh, J. & Saiyed, H. Determination of nicotine and cotinine in tobacco harvesters' urine by solid-phase extraction and liquid chromatography. *J. Chromatogr. B* **802**, 323–328 (2004).
10. Acosta, M. C., Buchhalter, A. R., Breland, A. B., Hamilton, D. C. & Eissenberg, T. Urine cotinine as an index of smoking status in abstinent smokers: Comparison of GC/MS with immunoassay test strip. *Nicotine Tob. Res.* **6**, 615–620 (2004).
11. Sun, J.-Y., Huang, K.-J., Wei, S.-Y., Wu, Z.-W. & Ren, F.-P. A graphene-based electrochemical sensor for sensitive determination of caffeine. *Colloids Surf. B Biointerf.* **84**, 421–426 (2011).
12. Mehmeti, E. *et al.* Wiring of glucose oxidase with graphene nanoribbons: An electrochemical third generation glucose biosensor. *Microchimica Acta* **184**(4), 1127–1134. https://doi.org/10.1007/s00604-017-2115-5 (2017).
13. Sundramoorthy, A. K. & Gunasekaran, S. Applications of graphene in quality assurance and safety of food. *TrAC Trends Anal. Chem.* **60**, 36–53 (2014).
14. Kumar, T. V., Yadav, S. K. & Sundramoorthy, A. K. Electrochemical synthesis of 2D layered materials and their potential application in pesticide detection. *J. Electrochem. Soc.* **165**, B848 (2018).
15. Lin, Y., Cui, X. & Ye, X. Electrocatalytic reactivity for oxygen reduction of palladium-modified carbon nanotubes synthesized in supercritical fluid. *Electrochem. Commun.* **7**, 267–274 (2005).
16. Rahman, M. M., Saleh Ahammad, A., Jin, J.-H., Ahn, S. J. & Lee, J.-J. A comprehensive review of glucose biosensors based on nanostructured metal-oxides. *Sensors* **10**, 4855–4886 (2010).
17. Mena, M., Yanez-Sedeno, P. & Pingarron, J. A comparison of different strategies for the construction of amperometric enzyme biosensors using gold nanoparticle-modified electrodes. *Anal. Biochem.* **336**, 20–27 (2005).

18. Teymourian, H., Salimi, A. & Hallaj, R. Low potential detection of NADH based on Fe3O4 nanoparticles/multiwalled carbon nanotubes composite: fabrication of integrated dehydrogenase-based lactate biosensor. *Biosensors Bioelectron.* **33**, 60–68 (2012).

19. Bharath, G. *et al.* Enhanced electrocatalytic activity of gold nanoparticles on hydroxyapatite nanorods for sensitive hydrazine sensors. *J. Mater. Chem. A* **4**, 6385–6394 (2016).

20. Devi, R. *et al.* Au/NiFe 2 O 4 nanoparticle-decorated graphene oxide nanosheets for electrochemical immunosensing of amyloid beta peptide. *Nanoscale Adv.* **2**, 239–248 (2020).

21. Afkhami, A., Soltani-Felehgari, F. & Madrakian, T. Gold nanoparticles modified carbon paste electrode as an efficient electrochemical sensor for rapid and sensitive determination of cefixime in urine and pharmaceutical samples. *Electrochimica acta* **103**, 125–133 (2013).

22. Arvand, M. & Dehsaraei, M. A simple and efficient electrochemical sensor for folic acid determination in human blood plasma based on gold nanoparticles–modified carbon paste electrode. *Mater. Sci. Eng. C* **33**, 3474–3480 (2013).

23. Saljooqi, A., Shamspur, T. & Mostafavi, A. The electrochemical sensor based on graphene oxide nanosheets decorated by gold nanoparticles and polythiophene for nicotine sensing in biological samples and cigarette. *J. Mater. Sci. Mater. Electron.* **31**, 5471–5477 (2020).

24. Jing, Y. *et al.* Determination of nicotine in tobacco products based on mussel-inspired reduced graphene oxide-supported gold nanoparticles. *Sci. Rep.* **6**, 1–8 (2016).

25. Majd, S. M., Salimi, A. & Astinchap, B. Label-free attomolar detection of lactate based on radio frequency sputtered of nickel oxide thin film field effect transistor. *Biosensors Bioelectron.* **92**, 733–740 (2017).

26. Liu, Y., Yuan, R., Chai, Y., Hong, C. & Guan, S. Preparation of a composite film electrochemically deposited with chitosan and gold nanoparticles for the determination of α-1-fetoprotein. *Bioprocess Biosyst. Eng.* **33**, 613–618 (2010).

27. Khezrian, S., Salimi, A., Teymourian, H. & Hallaj, R. Label-free electrochemical IgE aptasensor based on covalent attachment of aptamer onto multiwalled carbon nanotubes/ionic liquid/chitosan nanocomposite modified electrode. *Biosensors Bioelectron.* **43**, 218–225 (2013).

28. Kuralay, F., Vural, T., Bayram, C., Denkbas, E. B. & Abaci, S. Carbon nanotube–chitosan modified disposable pencil graphite electrode for Vitamin B12 analysis. *Colloids Surf. B Biointerf.* **87**, 18–22 (2011).

29. Tsai, Y.-C., Chen, S.-Y. & Liaw, H.-W. Immobilization of lactate dehydrogenase within multiwalled carbon nanotube-chitosan nanocomposite for application to lactate biosensors. *Sensors Actuators B Chem.* **125**, 474–481 (2007).

30. Zhang, Q., Chen, X., Tu, F. & Yao, C. Ultrasensitive enzyme-free electrochemical immunoassay for free thyroxine based on three dimensionally ordered macroporous chitosan–Au nanoparticles hybrid film. *Biosensors Bioelectron.* **59**, 377–383 (2014).

31. Zaki, M. *et al.* Mn/Cu nanoparticles modified carbon paste electrode as a novel electrochemical sensor for nicotine detection. *Electroanalysis* **35**, e202200143 (2023).

32. Zaki, M., Shafie, E. E., Abdel-Gawad, S. A., Fekry, A. M. & Shehata, M. Sensitive detection for nicotine using nickel/copper nanoparticle–modified carbon paste electrode. *Ionics* **28**, 4881–4891 (2022).

33. Chaki, N. K. & Vijayamohanan, K. Self-assembled monolayers as a tunable platform for biosensor applications. *Biosensors Bioelectron.* **17**, 1–12 (2002).

34. Shehata, M., Azab, S., Fekry, A. & Ameer, M. Nano-TiO2 modified carbon paste sensor for electrochemical nicotine detection using anionic surfactant. *Biosensors Bioelectron.* **79**, 589–592 (2016).

35. Farghali, R., Fekry, A., Ahmed, R. A. & Elhakim, H. Corrosion resistance of Ti modified by chitosan–gold nanoparticles for orthopedic implantation. *Int. J. Biol. Macromol.* **79**, 787–799 (2015).

36. Heakal, F.E.-T. & Fekry, A. Experimental and theoretical study of uracil and adenine inhibitors in Sn-Ag alloy/nitric acid corroding system. *J. Electrochem. Soc.* **155**, C534 (2008).

37. Abd El-Salam, H., Abd El-Hafez, G., Askalany, H. & Fekry, A. A creation of poly (N-2-hydroxyethylaniline-co-2-chloroaniline) for corrosion control of mild steel in acidic medium. *Jo. Bio- Tribo-Corros.* **6**, 1–14 (2020).

38. Kissinger, P. & Heineman, W. R. *Laboratory Techniques in Electroanalytical Chemistry, Revised and Expanded* (CRC Press, 2018).

39. Fekry, A. M. A new simple electrochemical Moxifloxacin Hydrochloride sensor built on carbon paste modified with silver nanoparticles. *Biosensors Bioelectron.* **87**, 1065–1070 (2017).

40. Li, X. *et al.* Graphene oxide orientated by a magnetic field and application in sensitive detection of chemical oxygen demand. *Analytica Chimica Acta* **1122**, 31–38 (2020).

41. Ravi, A. K., Punnakkal, N., Vasu, S. P. & Nair, B. G. Manganese dioxide based electrochemical sensor for the detection of nitro-group containing organophosphates in vegetables and drinking water samples. *J. Electroanal. Chem.* **859**, 113841 (2020).

42. Sun, C. *et al.* A chitosan-Au-hyperbranched polyester nanoparticles-based antifouling immunosensor for sensitive detection of carcinoembryonic antigen. *Analyst* **139**, 4216–4222 (2014).

43. Wang, Q., Moser, J.-E. & Grätzel, M. Electrochemical impedance spectroscopic analysis of dye-sensitized solar cells. *J. Phys. Chem. B* **109**, 14945–14953 (2005).

44. Kubendhiran, S. *et al.* Electrochemically activated screen printed carbon electrode decorated with nickel nano particles for the detection of glucose in human serum and human urine sample. *Int. J. Electrochem. Sci.* **11**, 7934–7946 (2016).

45. Zeng, Z., Zhou, H., Long, X., Guo, E. & Wang, X. Electrodeposition of hierarchical manganese oxide on metal nanoparticles decorated nanoporous gold with enhanced supercapacitor performance. *J. Alloys Compd.* **632**, 376–385 (2015).

46. Ahmed, R. A., Farghali, R. & Fekry, A. Study for the stability and corrosion inhibition of electrophoretic deposited chitosan on mild steel alloy in acidic medium. *Int. J. Electrochem. Sci* **7**, 7270–7282 (2012).

47. Mehmeti, E., Kilic, T., Laur, C. & Carrara, S. Electrochemical determination of nicotine in smokers' sweat. *Microchem. J.* **158**, 105155 (2020).

48. Brunet, B. R., Barnes, A. J., Scheidweiler, K. B., Mura, P. & Huestis, M. A. Development and validation of a solid-phase extraction gas chromatography–mass spectrometry method for the simultaneous quantification of methadone, heroin, cocaine and metabolites in sweat. *Anal. Bioanal. Chem.* **392**, 115–127 (2008).

49. Suffredini, H. B. *et al.* Electrochemical behavior of nicotine studied by voltammetric techniques at boron-doped diamond electrodes. *Anal. Lett.* **38**, 1587–1599 (2005).

50. Yang, S. & Smetena, I. Evaluation of capillary electrophoresis for the analysis of nicotine and selected minor alkaloids from tobacco. *Chromatographia* **40**, 375–378 (1995).

51. Shalaeva, M., Kenseth, J., Lombardo, F. & Bastin, A. Measurement of dissociation constants (pKa values) of organic compounds by multiplexed capillary electrophoresis using aqueous and cosolvent buffers. *J. Pharm. Sci.* **97**, 2581–2606 (2008).

52. Jiang, J. & Du, X. Sensitive electrochemical sensors for simultaneous determination of ascorbic acid, dopamine, and uric acid based on Au@ Pd-reduced graphene oxide nanocomposites. *Nanoscale* **6**, 11303–11309 (2014).

53. Yang, L., Wang, J., Lü, H. & Hui, N. Electrochemical sensor based on Prussian blue/multi-walled carbon nanotubes functionalized polypyrrole nanowire arrays for hydrogen peroxide and microRNA detection. *Microchimica Acta* **188**, 1–12 (2021).

54. Kunpatee, K. *et al.* A highly sensitive fenobucarb electrochemical sensor based on graphene nanoribbons-ionic liquid-cobalt phthalocyanine composites modified on screen-printed carbon electrode coupled with a flow injection analysis. *J. Electroanal. Chem.* **855**, 113630 (2019).

55. Sanati, A. L., Karimi-Maleh, H., Badiei, A., Biparva, P. & Ensafi, A. A. A voltammetric sensor based on NiO/CNTs ionic liquid carbon paste electrode for determination of morphine in the presence of diclofenac. *Mater. Sci. Eng. C* **35**, 379–385 (2014).

56. Roushani, M., Shamsipur, M. & Pourmortazavi, S. M. Amprometric detection of Glycine, l-Serine, and l-Alanine using glassy carbon electrode modified by NiO nanoparticles. *J. Appl. Electrochem.* **42**, 1005–1011 (2012).
57. Li, D. *et al.* Graphene-based nitrogen-doped carbon sandwich nanosheets: A new capacitive process controlled anode material for high-performance sodium-ion batteries. *J. Mater. Chem. A* **4**, 8630–8635 (2016).
58. Reddy, S. L., Arul, C., Zhaoqi, L., Lavanya, N. & Sekar, C. A novel electrochemical sensor based on Fe-doped MgNi2O3 nanoparticles for simultaneous determination of dopamine, uric acid, nicotine and caffeine over very wide linear ranges. *J. Electroanal. Chem.* **878**, 114648 (2020).
59. Yang, N., Wan, Q. & Yu, J. Adsorptive voltammetry of Hg (II) ions at a glassy carbon electrode coated with electropolymerized methyl-red film. *Sensors Actuators B Chem.* **110**, 246–251 (2005).
60. Wong, A., Scontri, M., Materon, E. M., Lanza, M. R. & Sotomayor, M. D. Development and application of an electrochemical sensor modified with multi-walled carbon nanotubes and graphene oxide for the sensitive and selective detection of tetracycline. *J. Electroanal. Chem.* **757**, 250–257 (2015).
61. Andrieux, C. & Savéant, J. Electron transfer through redox polymer films. *J. Electroanal. Chem. Interfac. Electrochem.* **111**, 377–381 (1980).
62. A.J. Bard, L.R. Faulkner, Fundamentals and Applications, New York: Wiley, 2001, in, Springer, 2002.
63. Haghshenas, E., Madrakian, T. & Afkhami, A. A novel electrochemical sensor based on magneto Au nanoparticles/carbon paste electrode for voltammetric determination of acetaminophen in real samples. *Mater. Sci. Eng. C* **57**, 205–214 (2015).
64. Benvidi, A. *et al.* Developing an electrochemical sensor based on a carbon paste electrode modified with nano-composite of reduced graphene oxide and CuFe2O4 nanoparticles for determination of hydrogen peroxide. *Mater. Sci. Eng. C* **75**, 1435–1447 (2017).
65. Fekry, A., Azab, S., Shehata, M. & Ameer, M. A novel electrochemical nicotine sensor based on cerium nanoparticles with anionic surfactant. *RSC Adv.* **5**, 51662–51671 (2015).
66. Meier, P. C. & Zünd, R. E. *Statistical Methods in Analytical Chemistry* (Wiley, 2005).
67. Geto, A., Amare, M., Tessema, M. & Admassie, S. Voltammetric determination of nicotine at poly (4-amino-3-hydroxynaphthalene sulfonic acid)-modified glassy carbon electrode. *Electroanalysis* **24**, 659–665 (2012).
68. Wu, C.-T., Chen, P.-Y., Chen, J.-G., Suryanarayanan, V. & Ho, K.-C. Detection of nicotine based on molecularly imprinted TiO2-modified electrodes. *Analytica Chimica Acta* **633**, 119–126 (2009).

## Author contributions

All the authors have contributed in making the experimental work, treating and analyzing the data and in writing and reviewing the manuscript.

## Funding

## Competing interests

The authors declare no competing interests.

## Additional information

**Correspondence** and requests for materials should be addressed to M.S.

**Reprints and permissions information** is available at www.nature.com/reprints.

**Publisher's note** Springer Nature remains neutral with regard to jurisdictional claims in published maps and institutional affiliations.